12th Symposium of Magnetic Measurements and Modeling SMMM'2016, Częstochowa–Siewierz, Poland, October 17–19, 2016

Magnetic Properties and Structure after Crystallization of $Fe_{80-x}B_{20}Nb_x$ ($x = 4$, 6, 10) Metallic Glasses

R. Nowosielski[a], M. Kądziołka-Gaweł[b], P. Gębara[c], D. Szyba[a] and R. Babilas[a,*]

[a]Institute of Engineering Materials and Biomaterials, Silesian University of Technology, S. Konarskiego 18a, 44-100 Gliwice, Poland

[b]Institute of Physics, University of Silesia, Uniwersytecka 4, 40-007 Katowice, Poland

[c]Institute of Physics, Częstochowa University of Technology, al. Armii Krajowej 19, 42-200 Częstochowa, Poland

The ferromagnetic Fe-based amorphous alloys were studied due to properties for soft magnetic applications. Depending on different Nb addition, the formation of crystalline phases after annealing of amorphous $Fe_{80-x}B_{20}Nb_x$ ($x = 4$, 6, 10) alloys was studied. The crystallization products as well as the phase structure were determined using the Mössbauer spectrometry combined with differential scanning calorimetry and magnetic measurements. The addition of Nb caused a shift of crystallization process towards higher temperatures and induced changes in coercive force and decreased the saturation magnetization. It was found that Nb addition changed the crystallization process from single crystallization for $Fe_{76}B_{20}Nb_4$ alloy to binary crystallization in the $Fe_{74}B_{20}Nb_6$ and $Fe_{70}B_{20}Nb_{10}$ glasses. The annealing process at the onset crystallization temperature induced complex phase formation including the α-Fe, Fe_3B, and Fe_2B phases for alloys $x = 4$, 6.

DOI: 10.12693/APhysPolA.131.1212

PACS/topics: 33.45.+x, 61.05.cp, 64.70.pe, 75.50.Kj

1. Introduction

In recent years a variety of ferromagnetic metallic glasses have been prepared extensively. The Fe-based glassy alloys have been mainly produced due to the attractive properties for magnetic applications. The required magnetic properties are usually large saturation magnetization, low coercive field and high magnetic permeability. Fe-based metallic glasses can be characterized by their chemical compositions containing metalloids (B, Si, P), other metals (Co, Ni, Cu, Zr, Hf, Mo, Nb, Al, Ta) and also rare earth elements [1–6].

The most important parameter during production of soft magnetic materials is the glass-forming ability (GFA), which defines a possibility of potential applications of manufactured products. The largest sample thickness, which can be obtained with a minimum cooling rate depends on the GFA. The thickness of conventional Fe-based glasses is around 0.3 mm, low GFA limits potential applications. However, Fe-based metallic glasses can be widely used as magnetic functional materials such as choke coils, transformer cores and sensors [7–10].

The Fe–B–Nb systems have rather good GFA, the addition of B up to 30 at.% enables the achievement of glassy alloys in bulk forms. Kaban et al. [11] studied the atomic structure of Fe–B–Nb glasses by reverse Monte Carlo simulation based on X-ray and neutron diffraction data in the case to explain the increase of the Curie temperature in the Fe–B–Nb ternary alloys with boron concentrations up to 30 at.%. The authors suggested that the increase of the Fe–Fe atomic pairs should explain the increase of the Curie temperature at constant niobium content. However, the Curie temperature decreases when Fe is replaced by niobium. This effect is related to the decrease of Fe–Fe distance and coordination numbers.

The magnetic properties of Fe–B–Y with Nb and Ti addition were measured in an area of saturation magnetization. Substitution of niobium by titanium improves the supercooled liquid region, which allows us to achieve high glass-forming ability with high magnetic saturation above 121 emu/g and high compressive strength about 3.4 GPa [10].

Torrens-Serra et al. [12, 13] studied $Fe_{65-x}Nb_{10}B_{25-x}$ ($x = 0$, 5, 10) and $Fe_{75-y}Nb_{9-y}B_{15}Cu_1$ ($y = 0$, 2, 4) metallic glasses in the form of ribbons prepared by a single-roller melt spinning. Authors revealed that studied ternary glasses can be assumed as good soft magnetic materials and glass-forming ability is improved with the increase of boron content. However, nanocrystallization of the studied alloys caused the increase of the coercive force. In the Fe–Nb–B–Cu system [13] the effect of replacing Nb by Fe and addition of Cu was also discussed. The addition of Cu leads to obtaining a refined microstructure with very tiny grains related to bcc-Fe crystalline phase which reduced a value of coercive force. What is more, the replacement of Nb by Fe decreased the thermal stability of amorphous structure, but improved a value of saturation magnetization and the Curie temperature.

The annealing process of Fe–Si–B and Fe–Si–B–Cu metallic glasses obviously caused their crystallization, but Nb addition in $Fe_{74.5}Si_{13.5}B_9Nb_3$ and $Fe_{73.5}Si_{13.5}B_9Nb_3Cu_1$ glasses stabilizes the amorphous structure, which can prevent crystallization and provides forming nanocrystals embedded in amorphous matrix [14].

*corresponding author; e-mail: rafal.babilas@polsl.pl

Based on above mentioned investigations, the aim of the present paper is to give information about the effect of Nb addition on magnetic properties and crystallization behavior of Fe–B–Nb alloys by using X-ray diffraction (XRD), differential scanning calorimetry (DSC), and vibrating sample magnetometer (VSM) methods. The study also presents results of crystalline phase analysis provided by the Mössbauer spectroscopy.

2. Experimental

The studies were performed on $Fe_{76}B_{20}Nb_4$, $Fe_{74}B_{20}Nb_6$, and $Fe_{70}B_{20}Nb_{10}$ metallic glasses in the form of ribbons with the thickness of 0.05 and the width of 6–8 mm. The master alloys were prepared by induction melting of a mixture of pure Fe (99.98%), B (99.9%), Nb (99.95%) in nominal compositions. The glassy ribbons were cast by the melt spinning method [15, 16]. The linear speed of copper wheel of 30 m/s and ejection over-pressure of molten ingot under Ar of 0.03 MPa were used as casting parameters.

The structure of the samples in the as-cast state was examined by XRD in reflection mode using the diffractometer with Co K_α radiation. The diffraction patterns for all samples were collected by the "step-scanning" method in the 2Θ range from 30° to 90°.

The crystallization study associated with the onset (T_x), the first and second peak crystallization (T_p) of studied samples were determined by the DSC method in the temperature range from 600 to 1100 K and a constant heating rate of 20 K/min under the argon atmosphere.

The ^{57}Fe Mössbauer spectra were recorded at room temperature using a constant acceleration spectrometer with triangular velocity shape, a multichannel analyzer with 1024 channels, and linear arrangement of the ^{57}Co(Cr) source (≈ 15 mCi), absorber and detector. The spectrometer velocity was calibrated with a high purity α-Fe foil. All spectra were fitted by means of a hyperfine field distribution using the Hesse–Rübartsch procedure with linear correlation between the isomer shift and hyperfine magnetic field. The numerical analysis of the Mössbauer spectra was performed with the use of the MOSS program.

Magnetic measurements of ribbons after annealing were carried out at room temperature by the LakeShore 7307 vibrating sample magnetometer in magnetic field up to 2 T. Study of magnetic properties included coercive force (H_c) and saturation magnetization (J_s), which were determined from hysteresis loops.

3. Results and discussion

The amorphous structure of Fe-based alloys in the as-cast state was confirmed by results of XRD investigations (Fig. 1). The diffraction patterns for $Fe_{80-x}B_{20}Nb_x$ (x = 4, 6, 10) show only broad peaks and diffuse halo patterns from 44° to 60° in the 2θ range for each alloy. No sharp peaks from crystalline phases are observed. The obtained results confirmed the amorphous structure of the studied alloy.

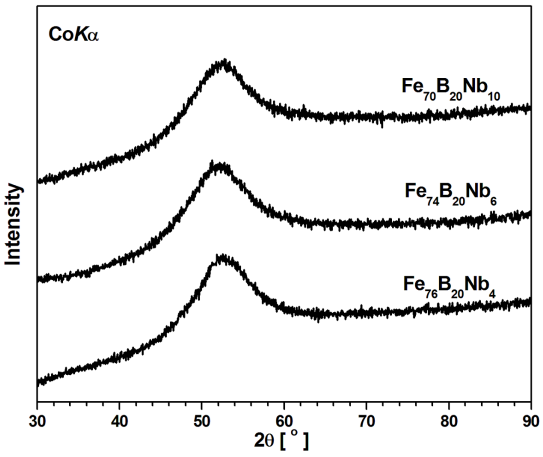

Fig. 1. X-ray diffraction patterns of Fe-based alloys in as-cast state.

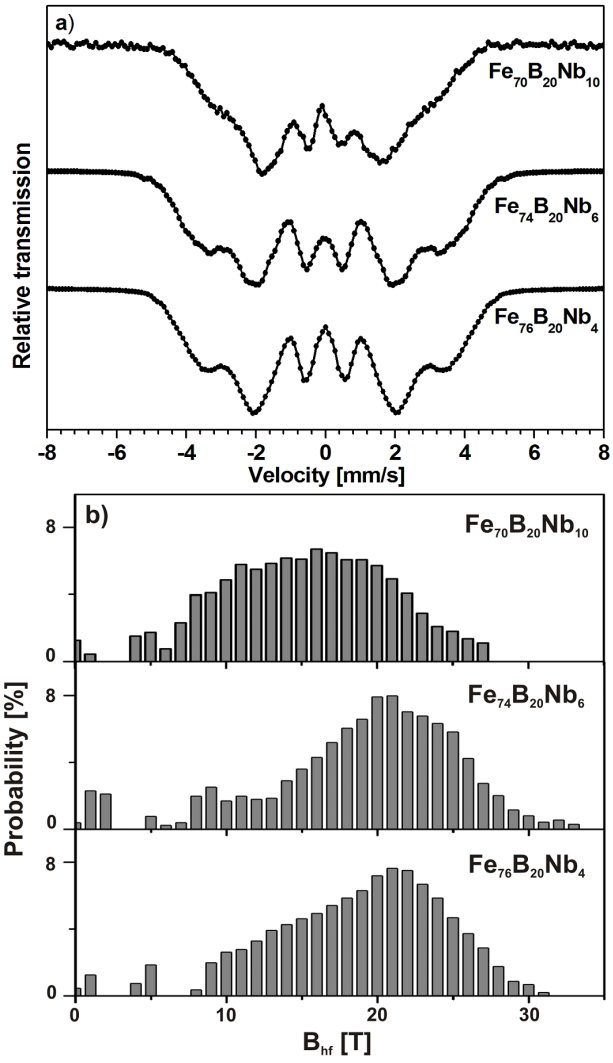

Fig. 2. Mössbauer spectra (a) with hyperfine magnetic field B_{hf} distributions (b) of studied Fe-based alloys in the as-cast state.

The room temperature Mössbauer spectra and hyperfine magnetic field (B_{hf}) distributions obtained for studied alloys in the as-cast state are presented in Fig. 2. The spectra show broadened sextet lines due to the atomic disorder of amorphous ferromagnetic materials. Moreover, a small asymmetry can be noticed. Also, the hyperfine magnetic field distributions are broad. This is connected with different local surroundings of the Fe atom in investigated alloys, which is characteristic for such materials. Together with increase of niobium concentration maximum of hyperfine magnetic fields distribution moves over in direction of smaller B_{hf}. Replacement of Fe atoms by Nb leads to changes in values of a hyperfine magnetic field of iron nuclides, for $Fe_{70}B_{20}Nb_{10}$ glass the lowest average value of $B_{hf} = 16.7$ T is determined. The average B_{hf} was 18.6 and 18.8 T for alloy with 4 and 6 at.% of Nb addition, adequately.

The DSC curves (Fig. 3) of studied glassy alloys present the exothermic peaks describing a single crystallization behavior observed for the $Fe_{76}B_{20}Nb_4$ sample and two-stage of crystallization for $Fe_{74}B_{20}Nb_6$ and $Fe_{70}B_{20}Nb_{10}$ glasses. The $T_x = 759$ K and $T_{p1} = 774$ K was achieved for the $Fe_{76}B_{20}Nb_4$ alloy. With the increase of Nb content, it can be observed that T_x gradually increases from 752 K for the $Fe_{76}B_{20}Nb_4$ alloy to 830 K for the alloy with 10 at.% of Nb addition. Similarly, the T_{p1} is also increased after iron replacing by niobium from 767 K for alloy with 6 at.% Nb to 840 K for glass with 10 at.% content of niobium. Moreover, for the $Fe_{70}B_{20}Nb_{10}$ metallic glass, the temperature of a second crystallization peak can be also designated ($T_{p2} = 1002$ K). Similarly, Torrens-Serra et al. [13] reported that the DSC heating caused the two-peak primary crystallization in the $Fe_{75}Nb_{10}B_{15}$ alloy and led to the formation of mainly the nanoscale bcc-Fe phase.

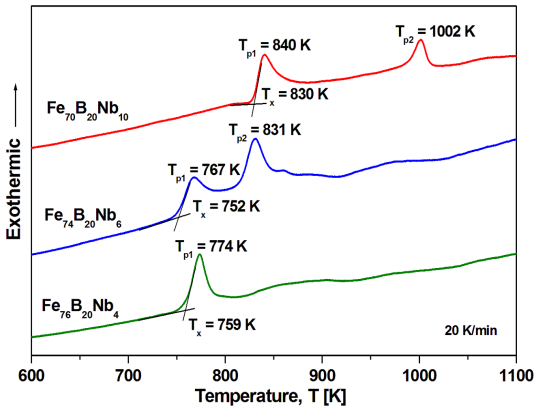

Fig. 3. DSC curves of Fe-based glassy ribbons in the as-cast state.

The Mössbauer spectra obtained for annealed samples at temperature near T_x were determined by DSC heating. The values of the hyperfine magnetic field as well as the isomer shift (IS) and relative area fraction of subspectra (A) are presented in Table I.

TABLE I

Hyperfine parameters of alloys annealed at 773 and 823 K/1 h (IS — isomer shift, B_{hf} — hyperfine magnetic field, A — relative area from the spectra). Experimental errors are smaller than 5%.

Alloy	IS [mm/s]	B_{hf} [T]	A [%]	Phase
$Fe_{76}B_{20}Nb_4$ 773 K/1 h	–0.076	22.5	18	Fe_2B
	0.084	24.0		
	0.188	22.3	53	Fe_3B
	0.075	26.5		
	0.113	28.6		
	0.004	33.2	29	α–Fe
$Fe_{74}B_{20}Nb_6$ 773 K/1 h	–0.05	13.5	19	Fe–B–Nb
	0.03	16.1		
	0.06	22.5	27	Fe_2B
	0.06	24.6		
	0.04	20.4	17	Fe_3B
	0.07	26.6		
	0.03	28.6		
	0.03	30.2	30	α-Fe
	0.01	33.0		
$Fe_{70}B_{20}Nb_{10}$ 823 K/1 h	–0.02	2.2	29	Fe-Nb
	–0.13	7.4	35	Fe-Nb
	0.12	11.7	33	Fe-B
	–0.05	32.0	3	α–Fe

The experimental spectrum of $Fe_{76}B_{20}Nb_4$ alloy after annealing at 773 K/1 h was fitted with six sextets, two corresponding to Fe_2B, three to Fe_3B, and one to α-Fe phase (Fig. 4a). Moreover, the spectrum of $Fe_{74}B_{20}Nb_6$ was fitted with nine sextets, two related to Fe_2B, three to Fe_3B and two to α-Fe phase (Fig. 4b). The spectrum obtained for $Fe_{70}B_{20}Nb_{10}$ sample after heat treatment at 823 K/1 h was fitted with four sextets, from which only one can be related to crystal phase α-Fe. Other three sextets visible on the Mössbauer spectrum of $Fe_{70}B_{20}Nb_{10}$ alloy are probably connected with amorphous fraction (Fig. 4c). Annealing at 823 K/1 h leads to some segregation of atoms in amorphous $Fe_{70}B_{20}Nb_{10}$. The sextets with hyperfine magnetic fields 2.2 T and 7.4 can be related with areas rich in Nb atoms and the sextet with $B_{hf} = 11.7$ T with part of sample rich in B atoms. The values of IS and B_{hf} for all sextets related to α-Fe phase can indicate that B and Nb atoms are also present in this structure.

As Zhang and Ramanujan [17] stated, iron replaced by niobium not only had a large effect on the crystallization temperature, but it also changed the magnetic properties. The saturation magnetization and the coercive force of studied Fe-based alloys after annealing at 373, 573, 773, and 823 K were measured by the VSM technique (Fig. 5). As is it can be observed, all the hysteresis loops exhibit the typical soft magnetic behavior. The samples present the highest saturation magnetization for alloys with 4 and 6 at.% of Nb addition in comparison with $Fe_{70}B_{20}Nb_{10}$ metallic glass.

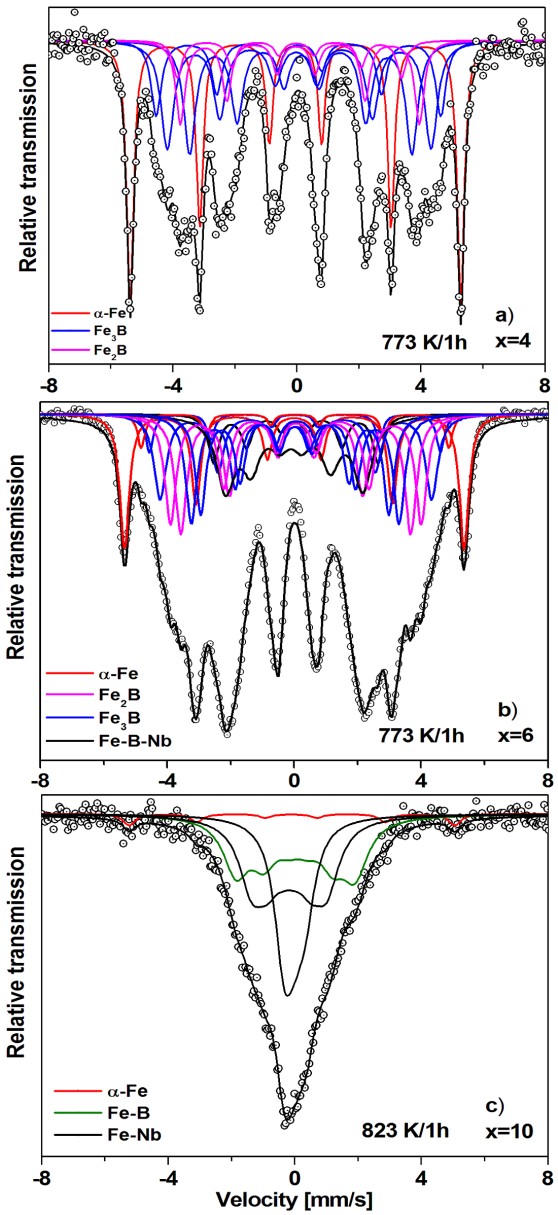

Fig. 4. Transmission Mössbauer spectra and fittings of $Fe_{80-x}B_{20}Nb_x$ alloy after annealing at 773 and 823 K/1 h: $x = 4$ (a), $x = 6$ (b), $x = 10$ (c).

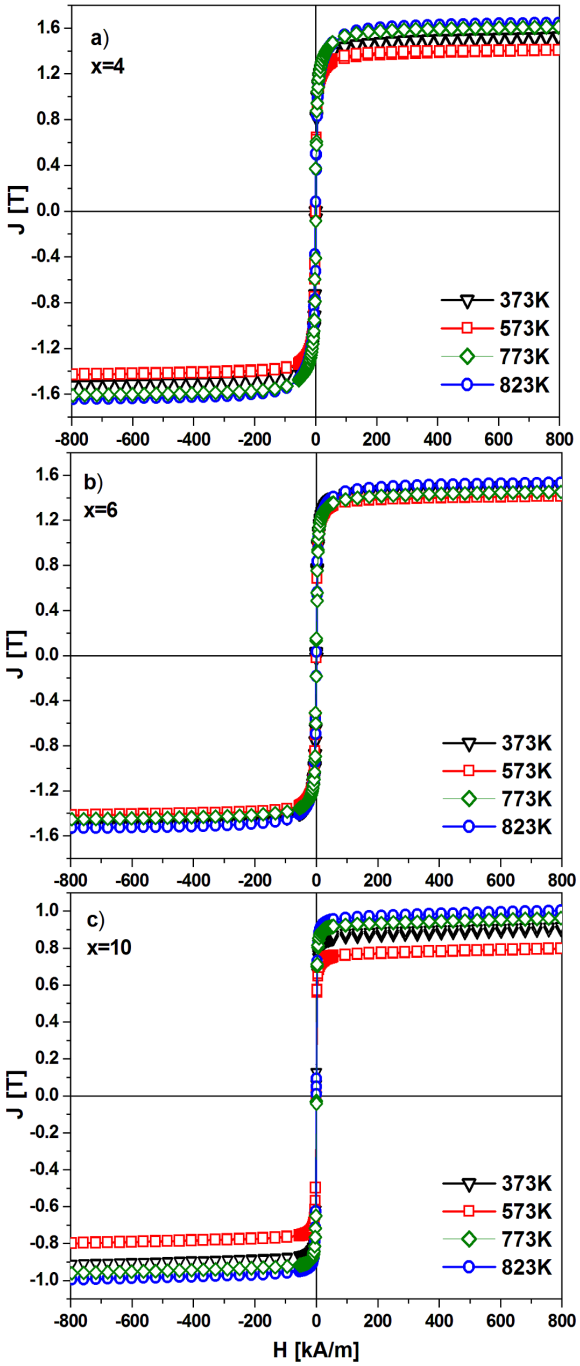

Fig. 5. The hysteresis loops of $Fe_{80-x}B_{20}Nb_x$ alloys in the form of ribbons after annealing at 373, 573, 773, 823 K/1 h: $x = 4$ (a), $x = 6$ (b), $x = 10$ (c).

The saturation magnetization of the $Fe_{80-x}B_{20}Nb_x$ alloy after annealing at 823 K is 1.63, 1.53, and 1.0 T for $x = 4$, 6, and 10, respectively. However, the coercive force for the same samples and the same heat treatment conditions is about 1.40, 1.31, and 0.28 kA/m, adequately. The significant increase of the coercivity for $Fe_{76}B_{20}Nb_4$ and $Fe_{74}B_{20}Nb_6$ alloys is due to the formation of the iron borides, which did not yet exist after annealing the $Fe_{70}B_{20}Nb_{10}$ ribbons at 823 K/1 h. Table II summarizes the magnetic properties for studied alloys.

4. Conclusions

The substitution of iron atoms in $Fe_{80-x}B_{20}Nb_x$ ($x = 4$, 6, 10) amorphous alloys by niobium atoms caused changes in the magnetic moment of Fe and consequently in magnetic saturation as well as coercive force. It was revealed that the niobium addition decreased the saturation magnetization for the same heat treatment condition. The DSC results show two distinct exothermic peaks in the $Fe_{74}B_{20}Nb_6$ and $Fe_{70}B_{20}Nb_{10}$ glass, however, only one peak is observed in the $Fe_{76}B_{20}Nb_4$ alloy. The annealing process provided near the onset crystallization temperature determined from DSC results al-

TABLE II

Magnetic properties of $Fe_{80-x}B_{20}Nb_x$ alloys (J_s — saturation magnetization, H_c — coercive force).

x [at.%]	T_a [K]	J_s [T]	H_c [A/m]
4	373	1.51	324
	573	1.41	196
	773	1.61	1181
	823	1.63	1398
6	373	1.52	220
	573	1.42	79
	773	1.45	1280
	823	15.3	1313
10	373	0.92	363
	573	0.80	87
	773	0.96	75
	823	1.00	281

lowed the formation of the α-Fe phase in all tested materials and also iron borides Fe_3B and Fe_2B in $Fe_{74}B_{20}Nb_6$ and $Fe_{76}B_{20}Nb_4$ alloys.

Acknowledgments

The work was supported by National Science Centre under research project no. 2011/03/D/ST8/04138. The authors thank P. Zackiewicz from Institute of Non-Ferrous Metals, Gliwice, Poland for help in the investigations.

References

[1] A. Inoue, B. Shen, A. Takeuchi, *Mater. Sci. Eng. A* **441**, 18 (2006).

[2] W. Yang, B. Sun, Y. Zhao, Q. Li, L. Hou, N. Luo, C. Dun, C. Zhao, Z. Ma, H. Liu, B. Shen, *J. Alloys Comp.* **676**, 209 (2016).

[3] H.Y. Jung, S.J. Choi, K.G. Prashanth, M. Stoica, S. Scudino, S. Yi, U. Kühn, D.H. Kim, K.B. Kim, J. Eckert, *Mater. Des.* **86**, 703 (2015).

[4] K. Suzuki, J.M. Cadogan, V. Sahajwalla, A. Inoue, T. Masumoto, *Mater. Sci. Eng. A* **226-228**, 554 (1997).

[5] A. Wang, C. Zhao, A. He, H. Men, C. Chang, X. Wang, *J. Alloys Comp.* **656**, 729 (2016).

[6] S. Meng, H. Ling, Q. Li, J. Zhang, *Scr. Mater.* **81**, 24 (2014).

[7] J. Zhang, C. Chang, A. Wang, B. Shen, *J. Non-Cryst. Solids* **358**, 1443 (2012).

[8] Q. Liu, J. Mo, H. Liu, L. Xue, L. Hou, W. Yang, L. Dou, B. Shen, L. Dou, *J. Non-Cryst. Solids* **443**, 108 (2016).

[9] J.F. Li, X. Liu, S.F. Zhao, H.Y. Ding, K.F. Yao, *J. Magn. Magn. Mater.* **386**, 107 (2015).

[10] H.B. Wang, L.X. Ma, L. Li, B. Zhang, *J. Alloys Comp.* **629**, 1 (2015).

[11] I. Kaban, P. Jóvári, A. Waske, M. Stoica, J. Bednarčik, B. Beuneu, N. Mattern, J. Eckert, *J. Alloys Comp.* **586**, S189 (2014).

[12] J. Torrens-Serra, J. Rodríguez-Viejo, M.T. Clavaguera-Mora, *J. Non-Cryst. Solids* **353**, 842 (2007).

[13] J. Torrens-Serra, P. Bruna, J. Rodriguez-Viejo, S. Roth, M.T. Clavaguera-Mora, *Intermetallics* **18**, 773 (2010).

[14] T. Alam, T. Borkar, S.S. Joshi, S. Katakam, X. Chen, N.B. Dahotre, R.V. Ramanujan, R. Banerjee, *AJ. Non-Cryst. Solids* **428**, 75 (2015).

[15] R. Babilas, M. Kądziołka-Gaweł, *Acta Phys. Pol. A* **127**, 573 (2015).

[16] R. Babilas, M. Kądziołka-Gaweł, A. Burian, L. Temleitner, *J. Magn. Magn. Mater.* **406**, 171 (2016).

[17] Y.R. Zhang, R.V. Ramanujan, *J. Alloys Comp.* **403**, 197 (2005).